THE BURNING OF LARGE N-HEPTANE DROPLETS IN MICROGRAVITY

Samuel L. Manzello and Mun Young Choi
Department of Mechanical Engineering
University of Illinois at Chicago
Chicago, IL 60607, USA

Andrei Kazakov and Frederick L. Dryer
Department of Mechanical and Aerospace Engineering
Princeton University
Princeton, NJ 08544

Ritsu Dobashi and Toshisuke Hirano
Department of Chemical System Engineering
The University of Tokyo
Tokyo, Japan

Keywords: Droplet combustion, microgravity combustion, sooting, radiation and laser diagnostics

Word Count (Wordperfect): 5877, **Total;** 3877, **Text**; 2000, 8 regular figures (1600) and 1 large figure (400)

Colloquium: Spray and Droplet Combustion

Choice of Presentation: Oral Presentation

Corresponding Author: Mun Young Choi
Department of Mechanical Engineering (M/C 251)
University of Illinois at Chicago
842 W. Taylor Street, Chicago, IL 60607
(312)996-7389, (312)413-0447 Fax
Munychoi@uic.edu

ABSTRACT

Experimental results are presented on the burning and sooting behavior of large n-heptane droplets in air at atmospheric pressure under microgravity conditions. The experiments were performed at the Japanese Microgravity Center (JAMIC) 10 sec dropshaft in Hokkaido, Japan. Soot volume fraction, burning rate, flame standoff and luminosity were measured for droplets of 2.6 mm and 2.9 mm in initial diameter. These are the largest droplets for which soot volume fraction measurements have ever been performed. Previous measurements of soot volume fractions for n-heptane droplets, confined to smaller droplet sizes of less than 1.8 mm, indicated that maximum soot volume fraction increased monotonically with initial droplet size. The new results demonstrate for the first time that sooting tendency is reduced for large droplets as it has been speculated previously but never confirmed experimentally. The lower soot volume fractions for the larger droplets were also accompanied by higher burning rates. The observed phenomenon is believed to be caused by the dimensional influence on radiative heat losses from the flame. Numerical calculations confirm that soot radiation affects the droplet burning behavior.

INTRODUCTION

Single, isolated droplet combustion experiments performed in microgravity provide an ideal environment to advance the understanding of diffusion flames. The absence of buoyancy results in a spherically-symmetric diffusion flame and measurements can be used to validate theories based on one-dimensional analysis. Although the simple d^2-law formulation [1,2] was quite successful in predicting many of the global parameters characterizing the droplet combustion process such as burning rate and flame standoff ratio, its deficiency was also very apparent in light of the theoretical and experimental evidence. In particular, n-heptane droplet flames exhibit significant sooting behavior, which was not considered in the classical analysis. Microgravity studies indicated that soot formation can influence many of the droplet burning parameters including the burning rate [3-5].

Jackson and Avedisian [6] studied the burning of n-heptane droplets ranging from 0.4 to 1.1 mm in diameter under microgravity conditions. They reported an increase in sooting tendency based on visual observation of the opacity of the soot-containing region as a function of the initial droplet diameter, while the measured burning rate was found to decrease with increasing initial droplet diameter. The increase in sooting, speculated to be caused by the longer residence time available for the fuel vapor to pyrolyze and form soot, was believed to be the primary factor responsible for the burning rate reduction. Hara and Kumagai [7, 8] also performed n-heptane microgravity experiments varying the initial droplet diameter from 0.6 to 1.1 mm but found only a weak effect of the initial diameter on the burning rate.

Choi *et al.* [9,10] first measured soot volume fraction for n-heptane droplets burning under microgravity conditions using light extinction technique for droplet size ranging from 0.8 to 1.8 mm in the 2.2 second droptower at the NASA Glenn Research Center (NASA-GRC). It was

demonstrated that the degree of sooting increases with initial droplet diameter. As the initial droplet size increases, the spatial extent of the flame which is proportional to droplet size prolongs the residence time of fuel vapor within the high-temperature environment. The reduction in the measured burning rate with initial droplet diameter correlated well with the increase in soot volume fraction. Soot formation is believed to influence the burning rate through (1) changes in thermophysical properties since sootshell serves as a heat sink, (2) physical barrier effects as sootshell can reduce fuel mass flux, and (3) through reduction in the effective heat of combustion. Furthermore, radiative heat losses can reduce the amount of heat that would otherwise be used to vaporize the fuel, subsequently leading to burning rate reduction. The results of Lee *et al.* [10] suggest that sooting and radiation effects will be more profound for larger droplets. However, the duration of the microgravity observation time available in the 2.2 sec droptower was insufficient to extend the investigation for larger droplets. Larger droplets require longer preparation time for droplet formation, deployment, ignition, and the oscillation decay period caused by these procedures.

Dietrich *et al.* [11] performed the first alkane droplet combustion experiments in space-based platforms aboard the Shuttle Columbia as part of STS-73 in 1995 using 60% heptane and 40% hexadecane droplets. Droplets with initial diameters of 3.5 and 5.2 mm were supported using 80μm silicon carbide fibers. In these experiments, the droplet flames exhibited a dim blue color instead of the bright luminous yellow observed for smaller droplets in ground-based studies [4], and no sootshells were observed to form around the droplet. Late in the burning period, the combustion chamber filled with "smoke" obscuring further visual observations. Based on the differences between these large droplet results and the data obtained for smaller droplets from ground-based studies, Dietrich *et al.* [11] recommended further investigations.

Nayagam *et al.* [12] recently performed unsupported droplet combustion experiments aboard the Space Shuttle Columbia as part of STS-94 using n-heptane droplets ranging from 1.7-4.1 mm. The motivation for these experiments was to gain new insights regarding the differences between the diffusive and radiative extinction of droplet flames. In these experiments, O_2-He mixtures were selected since He-diluent environments are known to reduce sooting as compared to N_2-O_2 systems [13]. In these large droplet experiments, soot production appeared to cease once the droplet diameter reached a "critical value". Relative soot concentrations were only estimated in this study based on visual analysis of high-speed photographs of the soot-containing region taken using backlighting. Backlighted analysis can suffer from saturation of the image [13] and can provide only qualitative information regarding sooting behavior. However, the droplet flames for very large droplets were also light blue, showing no presence of soot radiation. It has been suggested that, for very large droplet sizes, flame temperature is sufficiently suppressed by non-luminous radiative losses so that soot cannot be formed [14]. However, there has been no quantitative confirmation of this speculation.

Considering the discrepancies in conclusions reached in different studies and lack of quantitative soot measurements for larger droplets, the effect of initial droplet diameter on droplet burning rate and sooting tendency remains to be fully established. In the present study, the quantitative droplet burning and soot volume fraction measurements performed previously only for small droplets [10] were extended to larger droplet sizes. The experimental data are compared with numerical analysis using a detailed computational model which includes consideration of both non-luminous and luminous (soot) radiative effects.

EXPERIMENT DESCRIPTION

Experiments were performed at the JAMIC dropshaft in Hokkaido, Japan. The JAMIC facilityis the longest dropshaft in the world and provides 10 seconds of gravity levels less than 10^{-5}g. The experimental apparatus (see Fig. 1) is a completely reconstructed version (different from the apparatus used by Choi and coworkers [9,15,10] to fit the smaller experimental bus of the JAMIC facility. The operating procedures, however, are similar to the previous experiments and the reader is referred to detailed descriptions available elsewhere [9,15,10].

For the soot light extinction measurements, light from a 635 nm diode laser attached to a single fiber optic cable was expanded to a diameter of 50 mm. The beam was collimated and directed through the top optical port of the 12 liter stainless steel combustion chamber, focusedusing a 200 mm focal length plano-convex lens and reflected using a second mirror positioned at 45°. The reflected beam was then imaged through a spatial filter to a high resolution CCD camera. Soot volume fraction distributions were obtained byapplying a 3-pt Abel inversion to the projected light extinction measurements [16,9,10]. Droplet diameter was measured by digitizing the laser backlit image of the droplet as a function of time and applying a non-subjective image processing technique to determine the threshold which separates the droplet from the background. The burning rate was obtained from a linear fit to the evolution of the square of the droplet diameter with time after the transient heat-up period. Flame emission was measured using a CCD camera equipped with a narrow band filter (Full-width-half-maxof 25 nm) with central wavelength equal to 700 nm. Flame intensity was measured by digitizingflame images and intensityprofiles were obtained through a vertical chord passing through the center of the droplet. The video outputs from all of the cameras were recorded using 3 separate Sony 8 mm recorders that were attached to the experiment bus.

RESULTS AND DISCUSSION

Figure 2 displays the laser-backlit images of soot-containing region as a function of time after ignition. The droplets were tethered using an 80 micron silicon carbide fiber. The fibers were used to prevent drifting of the droplet out of the field of view during the observation period. After ignition, a spherical soot cloud was seen to form at approximately 0.2 s and soon developed into a spherical sootshell. A small soot-tail can be seen to form between 0.7 to 0.9 seconds, ostensibly caused by the slight residual motion in the gas-phase induced by the retraction of the igniter. Despite the formation of the soot-tail, symmetry of the sootshell is maintained in the bulk of the soot-containing region. The average velocity of the soot aggregates within the soot-tail is approximately 1 mm/s which is comparable to convection experienced by droplets burning in space-platform experiments [12].

The formation of soot-tails and the disturbance of the sootshell are more likely to occur for large droplets than small droplets. The main cause for this is that the balance between thermophoretic and Stefan velocities, which determines the location of the sootshell, is more precarious for the large droplets. The Stefan velocity is inversely proportional to the droplet diameter ($v_s \propto \frac{K}{d_o^2}$, where K is the burning rate and d_o is the droplet diameter). Reduction in v_s for larger droplets results in the soot standoff ratio (SSR) being established closer to the droplet surface. Figure 3 displays the measured soot standoff ratio (SSR) and the flame standoff ratio (FSR) for the 2.6 mm and 2.9 mm experiments along with previous results [6,10]. As shown in the figure, both SSR and FSR decrease as the initial droplet diameter is increased. The reduction in the SSR suggests that the thermophoretic

flux is less affected compared to Stefan flux as the droplet size is increased. Even though reduction in the flame temperature is expected for larger droplets due to increased radiative heat losses [14], the temperature gradient is compensated by the closer location of the flame relative to the droplet surface as shown by the smaller FSR values for the larger droplets.

The aggregates within the soot-tail region coagulate and attain dimensions on the order of hundreds of micrometers. The growth of the large aggregates may not be entirely induced by convection effects. Modeling results of Mackowski*et al.* [17] have suggested that radiative cooling of the soot particles can accelerate the growth of large aggregates through increases in the collision frequency caused by thermophoretic transport. If the growth of the large aggregates is primarily through agglomeration of existing soot particles rather than through surface growth through the addition of gas-phase species, then this mechanism will act as a sink for soot concentration in the vicinity of the large aggregates. Previous experiments on large (up to 4 mm initial diameter) n-heptane droplets burning in O_2-He environments have observed significant reductions in the opacity of the soot-containing region after the formation of large aggregates [12]. The viscous drag (caused by Stefan flux) can no longer be balanced by thermophoresis under these situations and the particles are transported towards the flame to be oxidized [18].

The soot volume fraction distributions were obtained for the 2.6 mm and 2.9 mm droplet along various directions for burning times prior to the disruption of the sootshell caused by the formation of the soot-tail. Figure 4 displays values obtained for the 2.9 mm experiment along the vertical direction. It is shown that the peak soot volume fraction gradually increases, reaches a maximum value and then decreases with time. This behavior is similar to that observed in small droplet experiments performed in the NASA droptower facility [9,10]. It is important to note that

the peak soot volume fraction reached its maximum prior to the formation of the large soot aggregates and disturbance due to the soot-tail formation. The influence of the asymmetry caused by the formation of the soot-tail was investigated by calculating the soot volume fraction at different angular positions. Soot volume fraction distributions were obtained and the average of the $f_{v,\,max}$ along the directions corresponding to θ = 135°, 20°, 0°, -45°, -160° and -180°, where θ is defined in Fig. 2., was calculated. The average $f_{v,max}$ values for the 2.6 mm and 2.9 mm initial droplet size cases were 34.5 and 37.6 ppm, respectively. These values are plotted versus the initial droplet diameter in Figure 5 along with previous measurements for smaller droplets from Lee *et al.* [10]. The maximum soot volume fractions for the larger droplets exhibit a significant departure from the linear increase as a function of d_0 as it might be inferred from the small droplet experiments. The measured maximum soot volume fractions for the larger droplets are nearly 40% smaller than the values obtained at d_0 = 1.8 mm. This reduction in sooting is expected to have strong implications on many aspects of the burning process.

Figure 6 displays the luminous flame images for the 2.9 mm droplet. The flame luminosity in gray levels was measured using a CCD camera equipped with a band-pass filter with a central wavelength of 700 nm and a FWHM of 25 nm. The intensity of the flame decreases dramatically with time. Despite the low flame luminosity, burning continued as evidenced by the nearly constant burning rate and the glow of the fiber in contact with the flame (see 1.0 s image in Fig. 6). The luminosity of the flame at this wavelength is primarily due to the presence of soot and its intensity is governed by local soot concentration and the temperature. Figure 7 displays the peak flame luminosity, the luminous flame radius, and $f_{v,max}$ as a function of the burning time for the 2.9 mm initial droplet size experiment. Previous experiments performed for smaller droplets indicated that the peak

flame luminosity increased to a maximum and then decreased with burning time. For the large droplets, the peak flame luminosity attains a maximum value just after ignition and decays at a rapid rate to undetectable levels at a time of approximately 1.5 sec. This dramatic reduction in flame luminosity is related to the soot concentration, flame size, and the flame temperature. The radiative emission is dependent on the volume and emissivity of the soot-containing medium. Since both the flame size and maximum soot concentration increase as a function of time, the rapid decay of the flame luminosity is primarily caused by reduction in the flame temperature.

Figure 8 displays the measured burning rates for the 2.6 mm and 2.9 mm experiments along with data measured by Lee *et al.* [10] for smaller droplets. The burning rate was calculated using the evolution of the square of the droplet diameter at fractional burning times (t/d_o^2) of approximately 0.25s/mm^2. For the smaller droplets, the burning rate decreases with increasing droplet size as a result of the sooting and attendant radiative heat losses [10]. The burning rates for the two large droplet experiments, 0.68 mm^2/s for the 2.6 mm droplet and 0.58 mm^2/s for the 2.9 mm droplet are significantly higher than the values that can be inferred based on trends from small droplet experiments.

To further elucidate the influence of soot radiation on the droplet burning behavior, a series of numerical simulations were performed. The computations were carried out using a moving finite-element chemically reacting flow model first described by Cho *et al.* [19]. The model simulates the transient spherically-symmetric combustion of a liquid droplet in an infinite oxidizing medium by solving the conservation equations of mass, species, and energy in both liquid and gas phases. Gas-phase chemistry of n-heptane oxidation was modeled with the semi-empirical reaction mechanism of Held *et al.* [20] that includes 275 reactions of 40 species. Radiative heat transfer was described

using a Planck-mean absorption formulation for both the gas-phase (non-luminous) and soot [21]. In the present work, the general analytical solution of the radiative heat transfer equation, originally obtained by Kuznetsov [22], was substituted for the formulation of Viskanta and Merriam[23] employed in a previous work [21]. The general analytical solution no longer imposes any limitations on the radial distribution of the Planck-mean coefficient, κ_p, while other derivatives of Kuznetsov's work found in the literature [23, 24] rely on the approximate solution that is based on the assumption of spatially-uniform κ_p. The Planck-mean absorption coefficient for non-luminous radiation due to CO, CO_2, and H_2O was calculated based on individual mole fractions [21]. The simulations were performed for the cases of no radiation (solid line), non-luminous radiation (dashed line), and non-luminous and soot radiation (open circle and solid line) contribution to the energy equation. The computed droplet burning rates for these cases are presented in Fig. 8 along with the experimental measurements. Figure 9a-c displays the predicted flame temperature distributions for the cases of no radiation (solid line), non-luminous radiation (dashed line), and non-luminous and soot radiation (streaked line) for $d_0 = 0.84$, 1.8, and 2.9 mm, respectively. For consistency with the experimental data reduction, the predicted burning rates were obtained from the linear fits to the computed square of the droplet diameter over a period of 1 s after ignition. As can be seen in Fig. 8, in the absence of radiation, the burning rate exhibits a relatively mild, linear dependence on the initial droplet diameter, a behavior that is caused by the increased influence of transient heating of the droplet interior [25]. As expected, the model prediction with no radiation significantly overpredicts the experimentally-measured burning rates. Inclusion of non-luminous radiation results in a considerable drop in the burning rate even for initial diameters below 1 mm (Fig. 8). This phenomenon is a result of the large volume of emitting components afforded by the large flame standoff distances [14]. With further

increase in the droplet size, the influence of radiation becomes more pronounced. For example, the maximum flame temperature for the case of $d_0 = 2.9$ mm is reduced by more than 600 K for the case of non-luminous radiation (Fig. 9, bottom panel), and the burning rate drops from 0.71 to 0.6 mm^2/s (Fig. 8). The computational results further indicate that accounting for the non-luminous radiation improves agreement between the model predictions and the experimental measurements by introducing a more rapid decrease (compared to the case of no radiation) of the burning rate with the initial diameter. However, the computed values generally overpredict the burning rate for droplet sizes larger than 1 mm. The contribution of soot radiative heat transfer was also included in the model by imposing the experimentally-measured soot volume fraction profiles available from Lee at al. [10] and the present work as a function of dimensionless radial distance for $d_0 = 0.84$, 1.8, and 2.9 mm (see Fig. 9a-c). The contribution of soot to the Planck-mean absorption coefficient was evaluated using [26]:

$$\kappa_{p,soot} = 3.83 \frac{K_e}{C_2} f_v T$$

where K_e is the dimensionless extinction constant dependent on soot refractive index and taken to be 8.5 [27], C_2 is 1.4388 cm-K, f_v is the local soot volume fraction, and T is the local temperature. The values of quasi-steady burning rates obtained from these calculations (open circles) and connected with interpolating line (solid line) are also presented in Fig. 8. The predicted burning rates are in good agreement with the experimentally observed trends. While quantitative agreement with the burning rate measurements for larger droplets has not been fully achieved (i.e., the burning rate for the case of d_0 = 2.9 mm is underpredicted by about 9%), the model captures the non-linear

dependence of the burning rate on the initial droplet diameter. The model predictions display a relatively weak effect of soot radiation on the burning rate at d_0 = 0.84 mm, but closely reproduces the rapid reduction in the burning rate for d_0 = 1.8 mm followed by a less prominent decrease for d_0 = 2.9 mm. It is also interesting to note that the effect of soot radiation on the flame structure appears to be much smaller than that of non-luminous radiation for all cases studied (Fig. 9a-c). This is due to the fact that the bulk of the soot resides within the lower temperature region of the sootshell rather than at the flame front.

The present modeling results strongly support the earlier proposals [10,14] that observed non-linear enhancement of the burning rate dependence on the initial droplet size is caused by soot and non-luminous radiation. It should be emphasized that detailed, transient modeling analysis with a kinetic model of soot formation (fully coupled with mass and energy balance in the system) will be required to fully elucidate the influence of sooting and radiation on droplet combustion. Although such work is currently in progress, it lies beyond the scope of the present study.

CONCLUSIONS

This study provides the first measurements of soot volume fractions for large n-heptane droplets burning under microgravity conditions. Soot concentration does not monotonically increase with d_o as inferred from small droplet experiments. The maximum soot volume fractions for the 2.6 mm and 2.9 mm droplets were nearly 40% lower than the values obtained for 1.8 mm droplet. The lower soot volume fractions were accompanied by higher burning rates and lower flame emissions. Numerical predictions indicate that the non-linear dependence of the droplet burning rate on the initial droplet diameter is caused by soot and non-luminous radiation.

ACKNOWLEDGMENTS

The authors gratefully acknowledge support through NASA (NCC3-655, Dr. P. Ferkul serving as project scientist) and to Mr. T. Sakuraya of the Japan Space Util. and Prom. Office. SLM acknowledges support from a NASA GSRP fellowship. The support of the JAMIC 10 sec. staff, NASA GRC staff (Mssrs. A. Birchenough, M. Johnston, C. Hampton, R. Mileto, J. Carrion, and J. Owens), and Dr. M. Suzuki of Nagaoka Univ. of Tech. is sincerely appreciated.

REFERENCES

1. Spalding, D.B., *Fourth Symp. (Intl) Combustion*, Williamsand Wilkins, Balt., MD, 1953, pp. 847-864.
2. Godsave, G.A.E., *Fourth Symp. (Intl) on Combustion* , Williams and Wilkins, Balt., MD, 1953, pp. 818-830.
3. Shaw, B.D., Dryer, F.L., Williams,F.A. and Haggard, Jr., J.B. *Acta Astronaut.* 17:1195-1120 (1988).
4. Choi, M.Y., Dryer, F.L. and Haggard, Jr., J.B., *Twenty-Third Symp. (Intl) Combustion,* The Comb. Inst., Pitts., PA, 1990, pp. 1597-1605.
5. Jackson, G.S., Avedsian, C.T. and Yang, J.C., *Int. J. Heat Trans.* 35:2017-2033 (1992).
6. Jackson, G.S. and Avedisian, C.T., *Proc. R. Soc. Lond. A* 446:255-275 (1994).
7. Hara, H. and Kumagai, S., *Twenty-Third Symp. (Intl) on Combustion*, The Comb. Inst., Pitts., PA, 1990, pp. 1605-1610.
8. Hara, H. and Kumagai, S., *Twenty Fifth Symp. (Intl) on Combustion*, The Comb. Inst., Pitts., PA, 1994, pp. 423-430.
9. Choi, M.Y. and Lee, K.O., *Twenty Sixth Symp. (Intl) on Combustion*, The Comb. Inst., Pitts., PA, 1996, pp.1243-1249.
10. Lee, K.O., Manzello, S.L., and Choi, M.Y., *Combust. Sci. Tech.* 132:139-156 (1998).
11. Dietrich, D.L., Haggard, Jr., J.B., Dryer, F.L., Nayagam, V., Shaw, B.D., and Williams,F.A., *Twenty Sixth Symp. (Intl) on Combustion*, The Comb. Inst., Pitts., PA, 1996, pp. 1201-1207.
12. Nayagam, V., Haggard, Jr., J.B., Colantonio, R.O., Marchese, A.J., Dryer, F.L., Zhang, B.L. and Williams, F.A.,*AIAA J.* 36:1369-1378 (1998).
13. Choi, M.Y., Ph.D. Thesis, Dept. of Mech. & Aero. Engin., Princeton University, MAE-T1937, 1992.
14. Marchese, A.J., Dryer, F.L. and Nayagam, V., *Combust. Flame* 116:432-458 (1999).
15. Lee, K.O. and Choi, M.Y., *Int'l J. of Microgravity Sci. and Tech.* X/2:86-94 (1998).
16. Dasch, C.J., *Appl. Opt.* 31:1146-1152(1992).
17. Mackowski, D.W., Tassopoulos, M. and Rosner, D.E., *Aero. Sci. Tech.* 20:83-99 (1994).
18. Choi, M.Y., Dryer, F.L., Green, G.J., and Sangiovanni, J.J., AIAA Paper 93-0823 (1993).
19. Cho, S. Y., Yetter, R. A, and Dryer, F. L., *J. Comp. Phys.* 102:160 (1992).
20. Held, T. J., Marchese, A. J., and Dryer, F. L., *Combust. Sci. Tech.* 123:107-146 (1997).
21. Marchese, A. J. and Dryer, F. L., *Combust. Sci. Tech.* 124:371-402 (1997).
22. Kuznetsov, E. S., *Izvestiya Akademii Nauk SSSR (Seriya Geofizicheskaya)* 15:69-93 (1951).
23. Viskanta, R. and Merriam, R. L., *J. Heat Transfer* 90:248-256 (1968).
24. Choi, S., and Kruger, C. H., *Combust. Flame* 61:131-144 (1985).
25. Law, C. K., *Combust. Flame* 26:17-22 (1976).

26. Kent, J. H., and Honnery, D. R., *Combust. Flame* 79:287-298 (1990).
27. Choi, M.Y., Mulholland, G.W., Hamins, A. and Kashiwagi, T., *Combust. Flame* 102:161-169 (1995).

FIGURES

1. Schematic of microgravity droplet combustion experimental apparatus.
2. Photographs of the soot-containing region for a 2.9 mm droplet obtained from the laser back-lit view.
3. Flame standoff ratio and soot standoff ratio for various sized droplets: solid symbols - present work, open symbols - Jackson and Avedisian (1994).
4. Transient variation of the soot volume fraction as a function of radial distance normalized by the instantaneous droplet radius for the experiment with d_0 = 2.9 mm.
5. Maximum soot volume fraction as a function of the initial droplet diameter.
6. Sequence of flame images for the 2.9 mm droplet obtained from the 700 nm side camera
7. Flame standoff ratio, flame luminosity and maximum soot volume fraction as a function of time for the d_0 = 2.9 mm experiment.
8. Measured and predicted droplet burning rate as a function of the initial droplet diameter. Model predictions were obtained for a) no radiation, b) non-luminous radiation, and c) non-luminous and luminous (soot) radiation.
9. Computed temperature profiles and smoothed experimentally-measured soot volume fraction distributions taken at 0.7 (top and middle panels) and 0.7 (bottom panel) seconds after ignition.

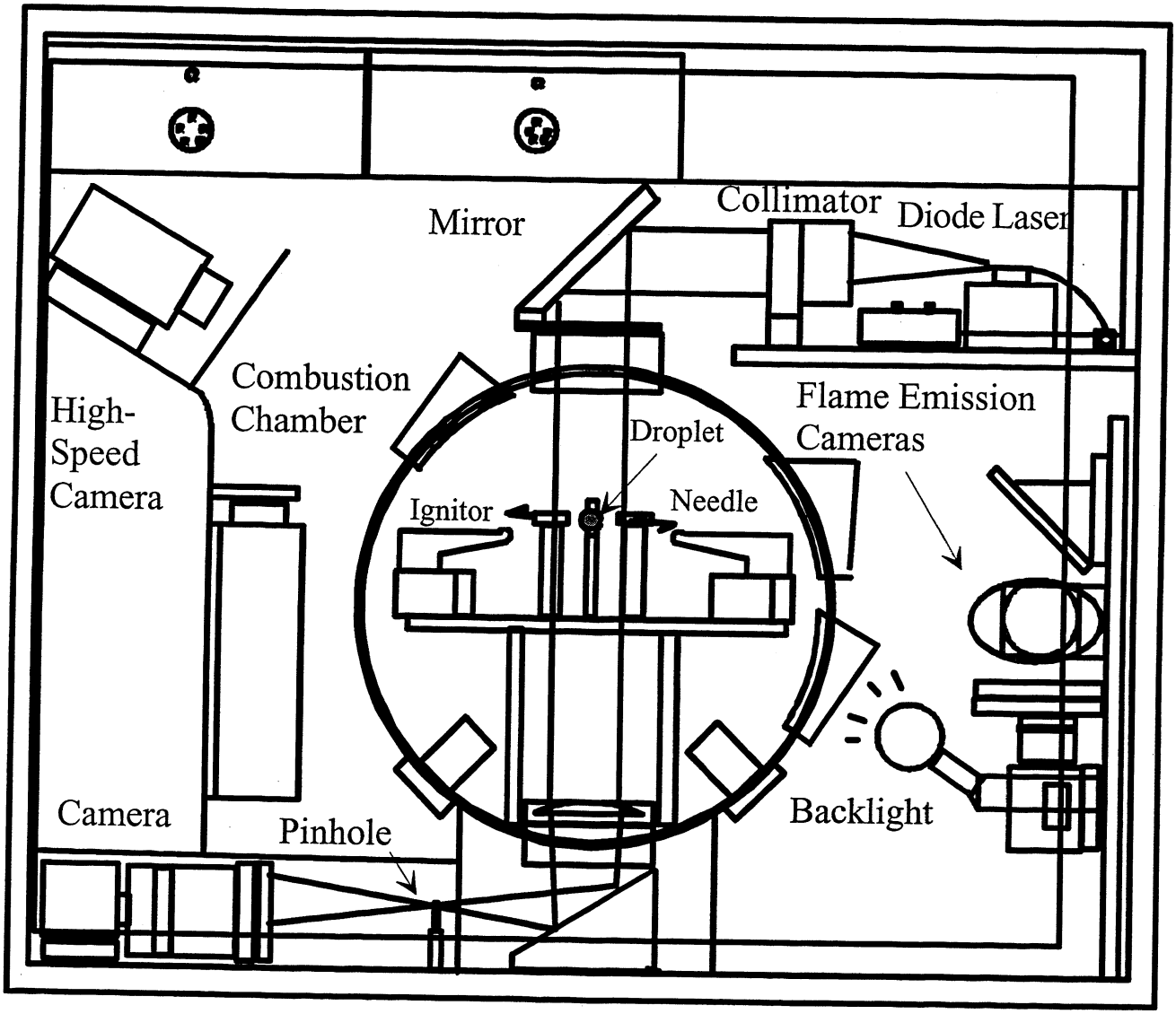
Mirror
Collimator
Diode Laser
Combustion Chamber
High-Speed Camera
Droplet
Ignitor
Needle
Flame Emission Cameras
Camera
Pinhole
Backlight

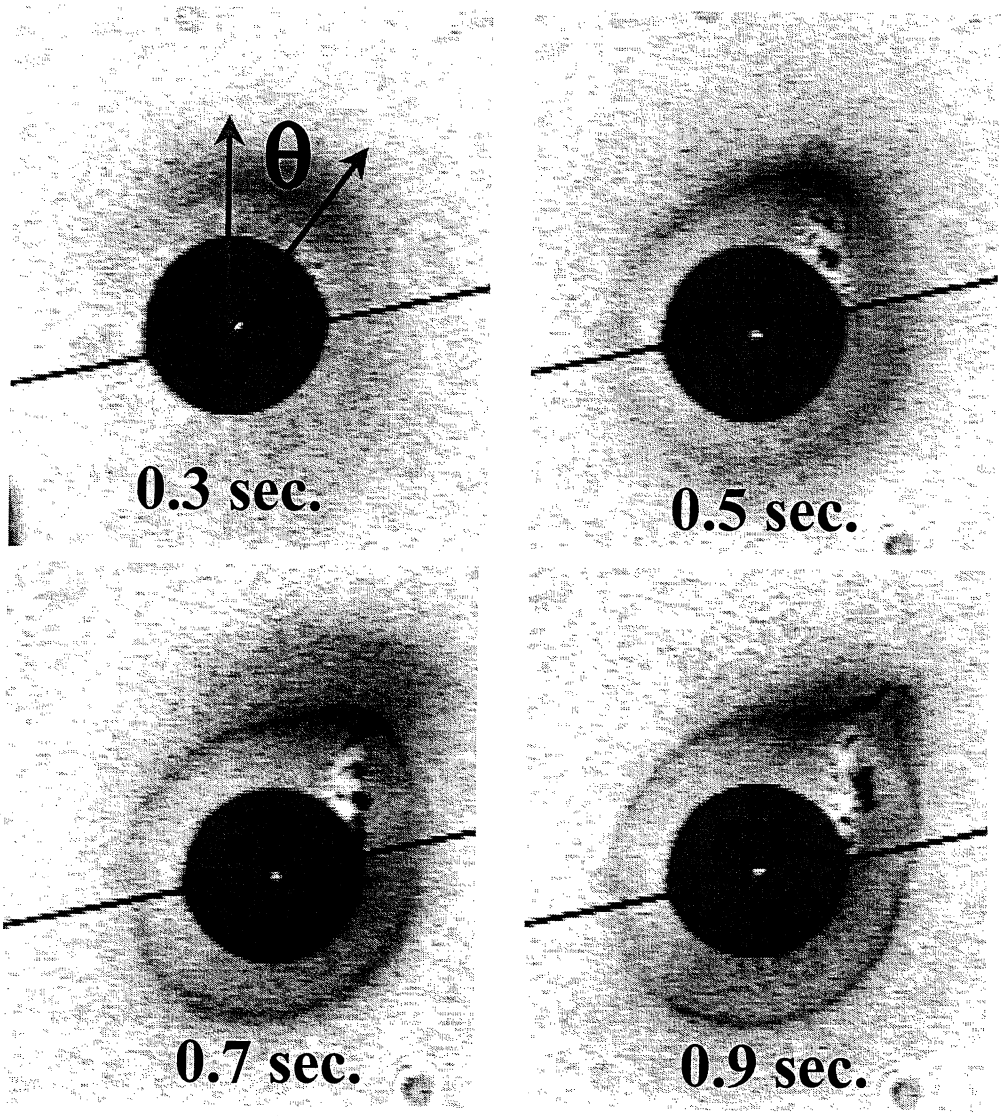
θ
0.3 sec.
0.5 sec.
0.7 sec.
0.9 sec.

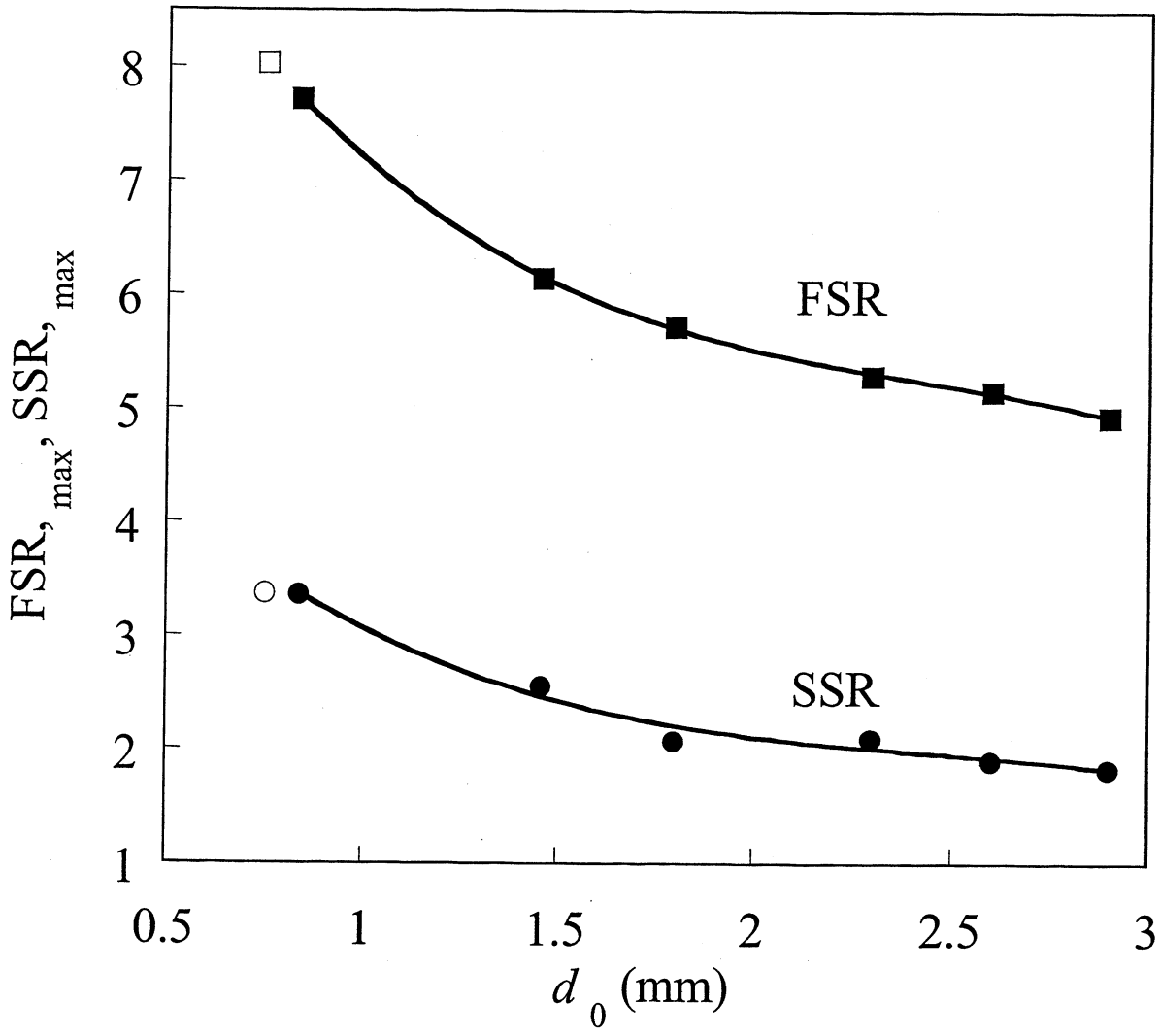
8
7
6
5
4
3
2
1
FSR, max, SSR, max
FSR
SSR
0.5
1
1.5
2
2.5
3
d 0 (mm)

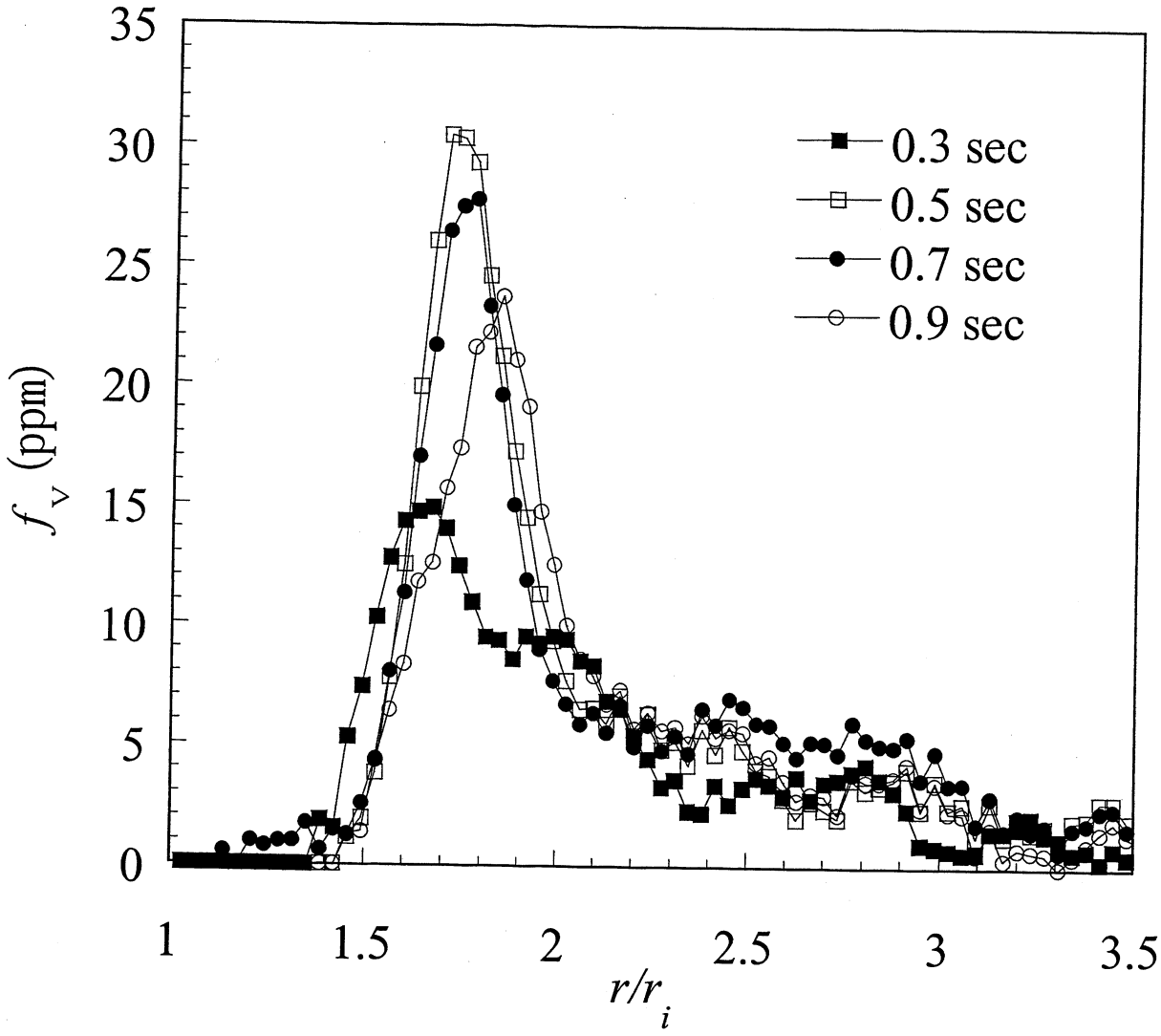
35
30
25
20
15
10
5
0
f_v (ppm)
1
1.5
2
2.5
3
3.5
r/r_i
0.3 sec
0.5 sec
0.7 sec
0.9 sec

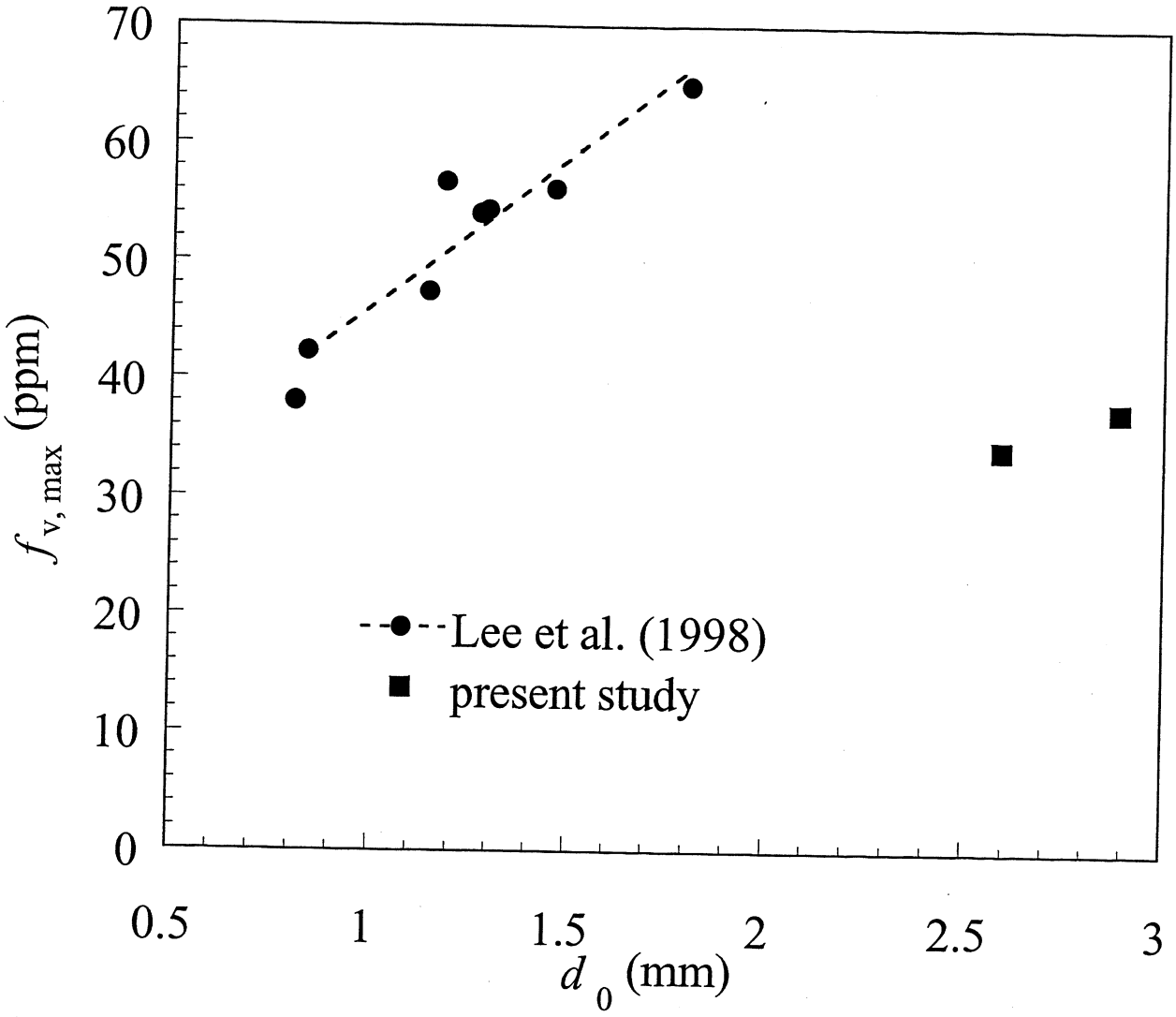
70
60
50
40
30
20
10
0
0.5
1
1.5
2
2.5
3
$f_{v,\,max}$ (ppm)
d_0 (mm)
Lee et al. (1998)
present study

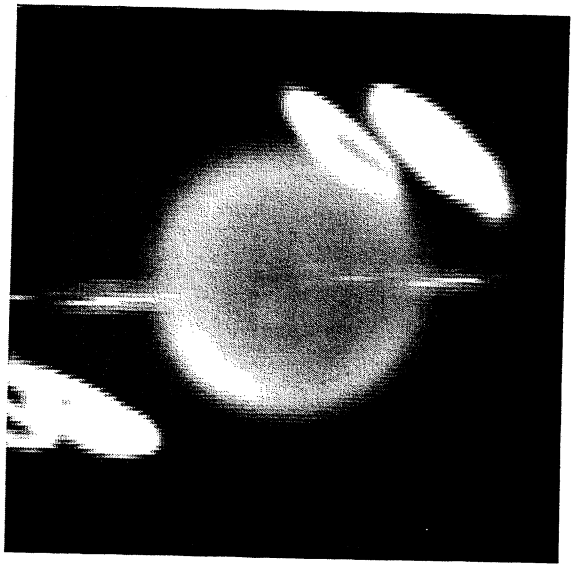

0.3 sec.

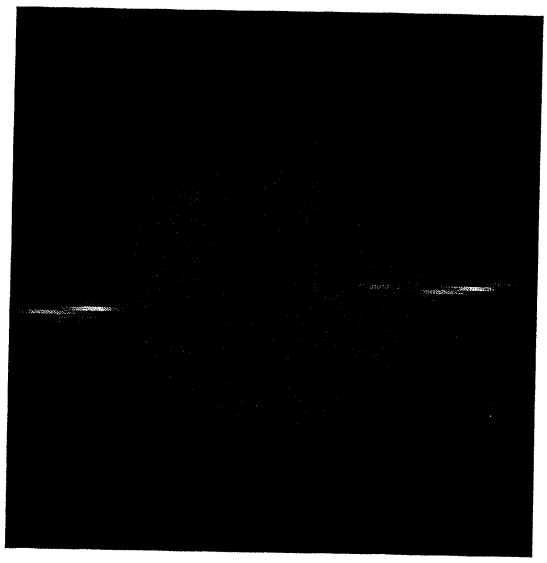

1.0 sec.

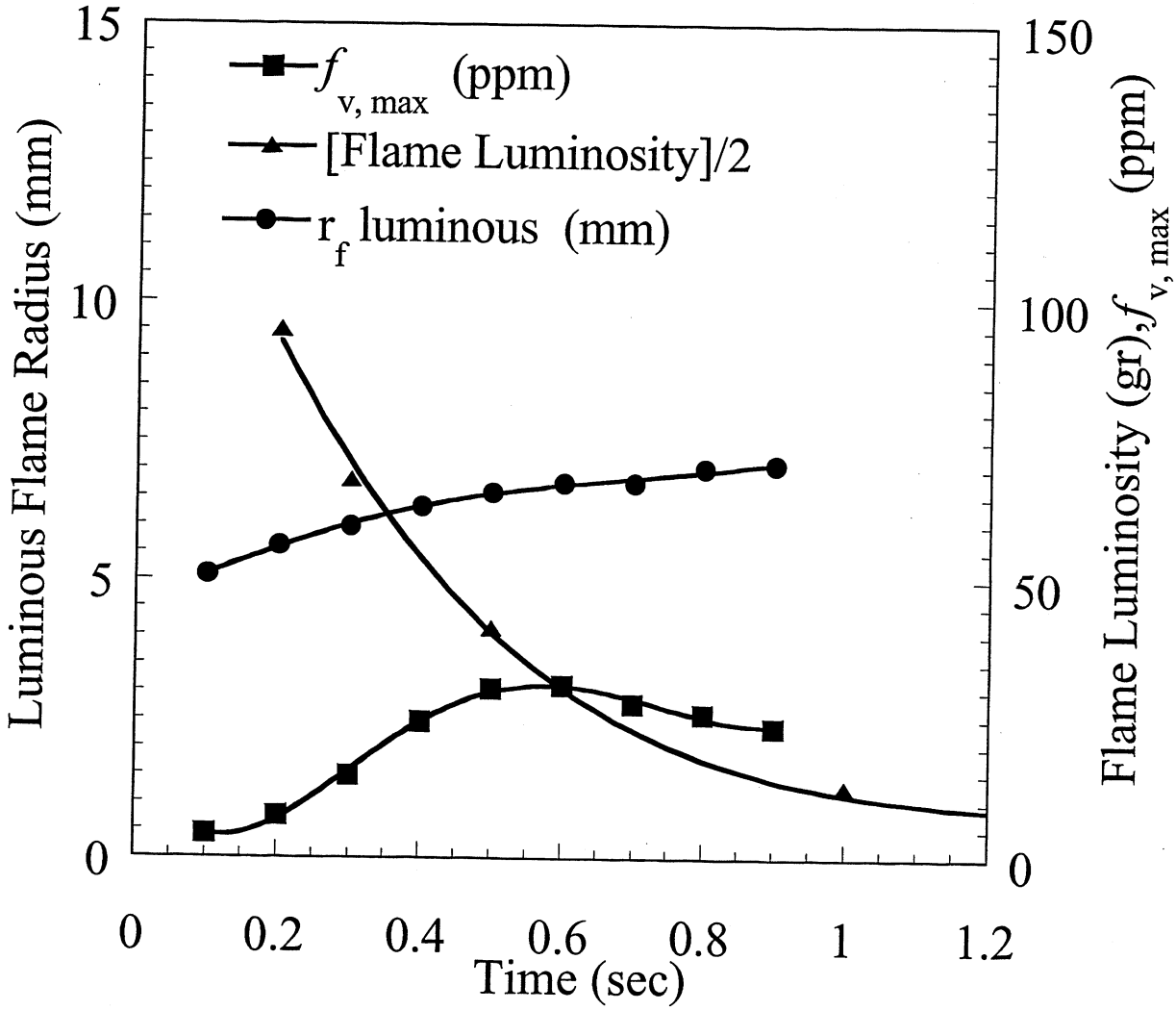
15
10
5
0
150
100
50
0
0
0.2
0.4
0.6
0.8
1
1.2
Time (sec)
Luminous Flame Radius (mm)
Flame Luminosity (gr), $f_{v, max}$ (ppm)
$f_{v, max}$ (ppm)
[Flame Luminosity]/2
r_f luminous (mm)

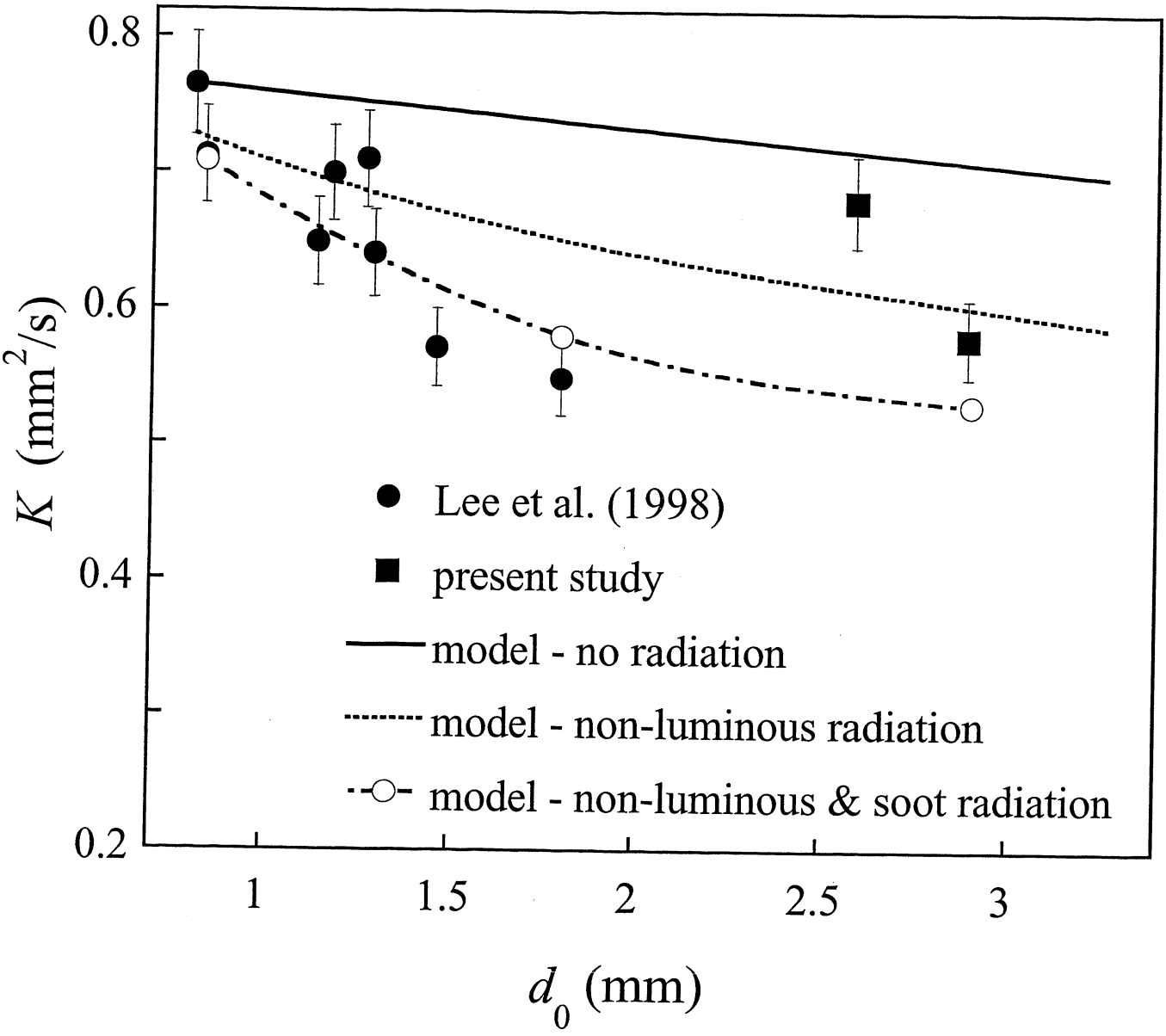
0.8
0.6
0.4
0.2
K (mm²/s)
1
1.5
2
2.5
3
d0 (mm)
Lee et al. (1998)
present study
model - no radiation
model - non-luminous radiation
model - non-luminous & soot radiation

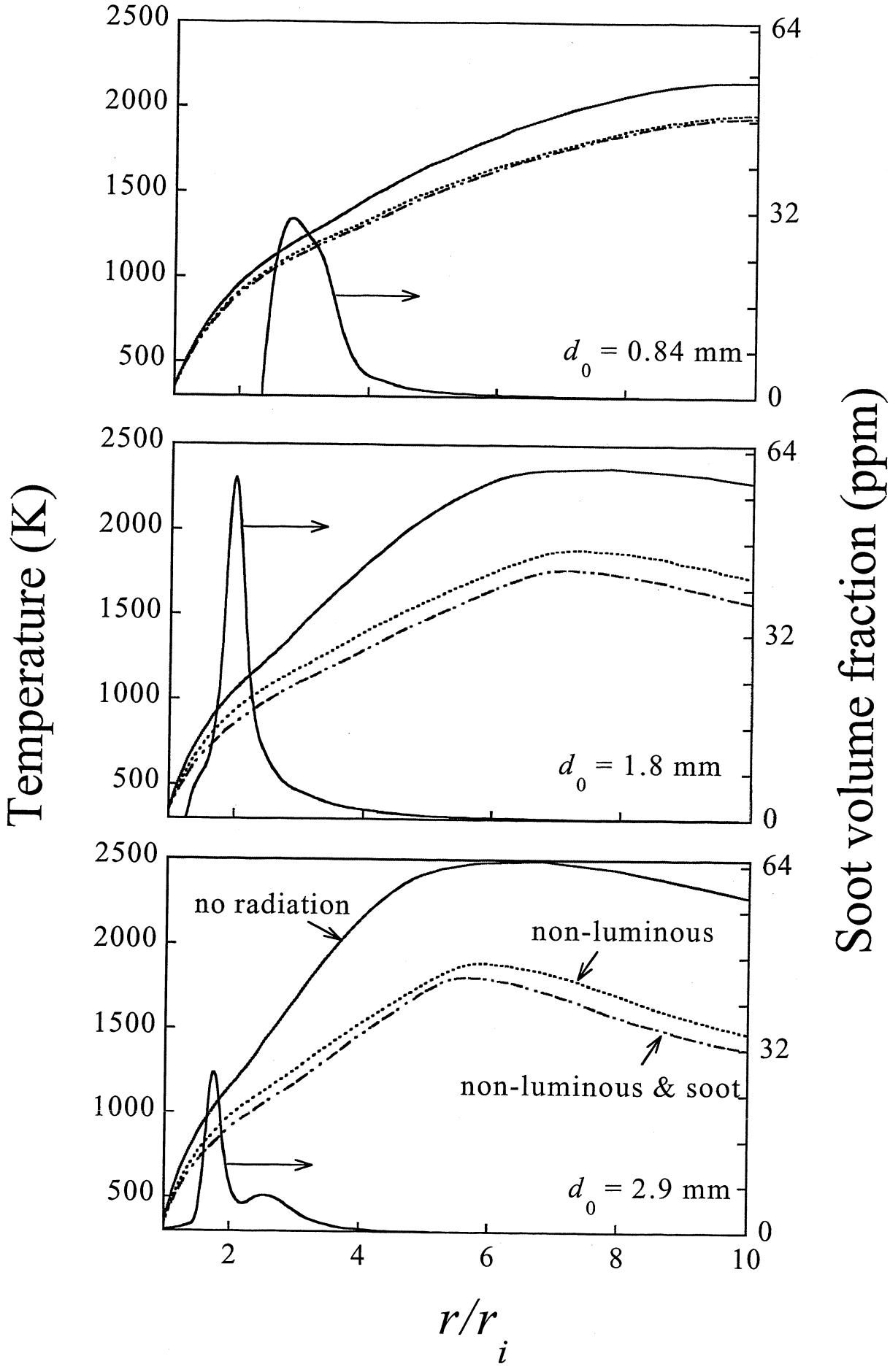
Temperature (K)
Soot volume fraction (ppm)
2500
2000
1500
1000
500
64
32
0
d_0 = 0.84 mm
d_0 = 1.8 mm
d_0 = 2.9 mm
no radiation
non-luminous
non-luminous & soot
2
4
6
8
10
r/r_i